Applied Energy 208 (2017) 1258–1273

Contents lists available at ScienceDirect

Applied Energy

journal homepage: www.elsevier.com/locate/apenergy

Numerical analysis of seawater desalination based on a solar chimney power plant

Tingzhen Ming[a,*], Tingrui Gong[b,**], Renaud K. de Richter[c], Cunjin Cai[a], S.A. Sherif[d]

[a] School of Civil Engineering and Architecture, Wuhan University of Technology, No. 122, Luoshi Road, Wuhan 430070, China
[b] Microsystem and Terahertz Research Center, China Academy of Engineering Physics, Chengdu 610200, China
[c] Tour-Solaire.Fr, 8 Impasse des Papillons, F34090 Montpellier, France
[d] Department of Mechanical and Aerospace Engineering, University of Florida, Gainesville, FL 32611, USA

HIGHLIGHTS

- Seawater droplets are sprayed for evaporation at the chimney inlet.
- 3D model was developed for the air cooling and condensation inside the chimney.
- The condensation level can be greatly reduced by the humidification.
- The humidification is conductive to improving the system desalination efficiency.

ARTICLE INFO

Keywords:
Solar chimney
Condensation
Water harvest from air
Desalination
Numerical simulation

ABSTRACT

In this paper, the desalination performance of a plant variant with the same size as the Manzanares pilot model was numerically investigated. A three-dimensional compressible flow and heat transfer model has been developed, describing the air cooling process along the chimney and the associated condensation. In this plant variant, instead of installing the turbine, water droplets were sprayed for evaporation at the bottom of the chimney, and thus airflow was subjected to humidification. Results show that with increased mass fraction of water in the air, the influence of the microclimate on the local environment will also increase. The evaporation of the droplets improves the relative humidity of the air within the chimney, and the condensation level can thus be greatly reduced. Moreover, the freshwater output increases with increasing amount of water sprayed, which is beneficial for the improvement of the desalination efficiency of the system.

1. Introduction

1.1. Background

The solar chimney power plant system (SCPPS) is a solar thermal application system to achieve output power, which has been verified and rapidly developed in recent years. In general, the system consists of four main components: a chimney, a collector, a thermal storage layer, and power conversion units (e.g. turbine generators). The main role of the collector is to harvest solar radiation to heat the air below. When the air density within the system is less than that of the ambient air at the same height, the system will produce a natural convection caused by buoyancy. Both the potential energy of the air and its thermal energy are converted into kinetic energy. The accumulated buoyancy causes a large pressure difference between the system and the ambient air. Because the chimney is erected in the middle of the collector, the heated air can rise through the chimney at a high speed. Turbine generators are located either at the bottom of the chimney or at the outlet of the collector (where there is a large pressure drop), thus converting the kinetic energy into electrical energy. The thermal storage layer enables electricity production after sunset.

1.2. Literature review

The idea of utilizing solar chimney technology to generate electricity was introduced by Professor Jörg Schlaich in the 1970s. In 1982, he built the world's first solar chimney pilot plant in Manzanares, Spain. The chimney had a height of 194.6 m, a diameter of 10.8 m, and a collector radius of 122 m. During the seven-year operation of the plant, it ran more than 95% of the expected time [1,2]. However, in 1986–1988 the annual

* Corresponding author.
** Corresponding author.
E-mail addresses: tzming@whut.edu.cn (T. Ming), gongtingrui@mtrc.ac.cn (T. Gong).

http://dx.doi.org/10.1016/j.apenergy.2017.09.028
Received 17 June 2017; Received in revised form 26 August 2017; Accepted 9 September 2017
Available online 20 September 2017
0306-2619/

Nomenclature

Ra	Rayleigh number
c_p	specific heat capacity [J/(K kg)]
L	characteristic length [m]
T	temperature [K]
u	velocity [m/s]
g	gravitational acceleration, 9.8 [m/s^2]
t	time [s]
S_m	mass source term [kg/(s m^3)]
S_F	momentum source term [N/m^3]
$coeff$	condensation coefficient
R_g	ideal gas constant [J/(kg K)]
R_s	water vapor gas constant [J/(kg K)]
Q_d	the amount of spray droplets [kg/s]
Q_{cons}	the condensed water [kg/s]
η_{cons}	condensation efficiency
p	pressure [Pa]
E	instantaneous energy inside the control volume [J]
k_{eff}	the effective conductivity [W/(m K)]
J	the diffusion flux of species
S_h	the heat of chemical reaction or any other volumetric heat sources [W/m^3]
h	sensible enthalpy [m/s^2]
Y	mass fraction of species
k	turbulence kinetic energy [J/kg]
G_k	the generation of turbulence kinetic energy due to mean velocity gradients [J]
G_b	the generation of turbulence kinetic energy due to buoyancy [J]
$C_{1\varepsilon}$, $C_{2\varepsilon}$, $C_{3\varepsilon}$	constants for turbulent model
S_{ct}	turbulent Schmidt number
S_{H2O}	water vapor added to or removed from the air [kg/(s m^2)]
D_{H2O}	diffusion coefficient of water vapor into air [m^2/s]
v	local air velocity [m/s]
q	the amount of injected water [kg/s]
h	convective heat transfer coefficient [W/(m^2 K)]
RH	relative humidity [%]

Greek symbols

Δ	difference or increase
α	thermal diffusivity [m^2/s]
β	thermal expansion coefficient [1/K]
ρ	air density [kg/m^3]
γ	latent heat of condensation [J/kg]
ε	turbulence kinetic energy dissipation rate [W/kg]
μ	dynamic viscosity [kg/(m s)]
μ_t	turbulent dynamic viscosity coefficient [kg/(m s)]
ν	kinematic viscosity [m^2/s]
σ_k	turbulent Prandtl number for k
σ_ε	turbulent Prandtl number for ε
τ	stress tensor [N/m^2]
Γ	diffusion coefficient
ϕ	scalar

Subscripts

i,j	any directions of x, y and z

average crude oil prices were nearly $15 nominal ($32 inflation adjusted price), as compared to $37 ($109 inflation adjusted) of the prices in 1980 [3], which resulted in reduced funding for research on solar energy and lack of maintenance of the guyed chimney, which collapsed in 1989 during a strong storm. Since then, the theoretical study of solar chimneys has attracted worldwide attention among researchers. Haaf et al. [1,2] provided experimental results and a scientific description of a solar chimney pilot plant. Zhou et al. [4,5] made a comprehensive overview of the scientific literature on solar chimney test power plants.

However, an unavoidable problem is that the overall efficiency of the SCPPS is relatively low, with nearly 3% in theory per 1 km height of chimney due to the Carnot cycle efficiency, but more or less only 1% can be achieved in reality due to frictions losses and components efficiency [6]. The overall efficiency of the SCPPS is affected by sunlight energy collection efficiency of the greenhouse, the ascending airflow efficiency of the chimney, the thermo-mechanical efficiency of the turbine, and the mechanical power of the generator [7]. Furthermore, the chimney plays an important role in improving the overall efficiency of the SCPPS: the higher the chimney, the higher the overall efficiency. The construction of the world's first large-scale SCPPS of up to 1000 m was planned to start in Mildura, Australia in 2002, with the support and significant attention of the federal government; the chief architect of this project was Professor Schlaich [8]. Pretorius and Backström [9,10] proposed the idea of building a SCPPS with a chimney height of 1500 m, and they also provided detailed calculations and structural designs. However, for the construction of such a high chimney, the economic costs and technical problems are formidable.

Encouragingly, researchers found the output performance of the SCPPS to be closely related to the ambient and operation conditions and structural dimensions, thus some optimization measures can help to increase the overall output power of the system.

Based on the establishment of a comprehensive mathematical model, a research group led by Prof. Sherif [11,12] analyzed the effects of parameters such as environmental conditions and structural dimensions on the temperature and output power of SCPPS. In addition, they built three different types of pilot plants in Florida, taking into account the chimney shape, the collector structure, and the performance of the thermal storage layer. Ming et al. [13] evaluated the performance of SCPPS via theoretical analysis and numerical validation. They used numerical models to study the effects of strong ambient crosswind [14] and chimney shape [15] on the heat transfer, air flow, and output power of SCPPS. Bernardes et al. [16] evaluated the effects of various environmental conditions and structural dimensions on the output power of SCPPS by establishing a numerical model. The results showed that the chimney height, the pressure drop factor of the turbine, the diameter of the chimney, and the optical properties of the collector were all important parameters that need to be considered for designing the SCPPS. Nizetic et al. [17] developed an analytical approach based on a simplified thermodynamic analysis of the overall SCPPS cycle, the optimum factors of the turbine pressure drop, which are important for the output power of SCPPS were investigated. Kratzig et al. [18] simulated the physical process of the SCPPS, demonstrated the efficiency of the system, and demonstrated its applicability in arid regions through two SCPPS optimization cases. Furthermore, they built a mathematical model to analyze the thermal-fluid mechanical processes within a SCPPS and evaluated the performance of the power generation system using output power as the indicator [7]. Shirvan et al. [19] investigated the effects of various parameters on the maximum potential power output of the SCPPS numerically, and their results indicated that the potential maximum power output increases with both chimney diameter and height, and decreases with increasing entrance gap of the collector. Patel et al. [20] studied the effect of geometric parameters on optimizing the structure of SCPPS. Maia et al. [21,22] established a numerical model of the internal turbulence of a solar chimney to assess the effect of geometric parameters and manipulated variables on fluid flow. The results showed that the height and diameter of the chimney

have the most significant effect on its flow characteristics. In addition, they also conducted the energy and efficacy analysis of the airflow within the solar chimney. Gholamalizadeh et al. [23] evaluated the influence of the site altitude on the performance of the SCPPS, and the authors found that the chimney diameter was the most important condition for the performance of the SCPPS. Hu et al. [24] raised some preliminary attributes of the novel controlling approach of the solar chimney system with variable diffuser outlet, and indicated that the diffuser-type solar chimney system had better performance than a cylindrical solar chimney.

However, drawing on these previous studies, if the SCPPS was solely used for power production, the energy conversion efficiency would still be relatively low (1% per km of chimney height), and the overall system output power would not be easy to improve. Therefore, at present many researchers working on solar chimney technology introduced some new solar chimney systems to improve the solar energy use efficiency.de Richter et al. [25] proposed to combine TiO_2 photocatalysis with SCPP to clean the atmosphere from of non-CO_2 greenhouse gases, thus helping to limit the global temperature rise. Gong et al. [26] proposed an inverted U-type solar chimney with a cooling tower system to reduce urban air pollution. Their system was equipped with a filter screen near the inlet of the collector and water was sprayed in the cooling tower to clean the air and to strengthen the system's natural flow. Zou et al. [27] proposed a hybrid cooling tower and a solar chimney concept that can simultaneously generate electricity and eliminate waste heat. Lee et al. [28] verified that it is feasible for solar chimneys to provide acceptable quality and quantity of heat for organic Rankine cycles. Ferreira et al. [29] studied the possibility of using a solar chimney to dry agricultural products. Li et al. [30] investigated the performance when phase change materials were applied to the solar chimney system and the results showed that it could extend the duration of the utilization of the solar chimney system. Ninic and Nizetic [31] studied the possibility of using warm wet air from the atmosphere by establishing a gravity vortex column model. Yu et al. [32] presented a coupled geothermal cooling system with an earth-to-air heat exchanger and a solar collector enhanced solar chimney to achieve free space cooling in summer.

Among these new solar chimney systems, Pretorius [10] and Kröger and Blaine [33] showed that the latent heat released by the wet air within the chimney may cause the output power of the SCPPS to increase in some specific atmospheric conditions. In addition, the moisture in the air should not evaporate in the collector, since the latent heat required for evaporation will reduce the power output. As a result, the air temperature inside the collector will drop [34]. Therefore, agricultural practices are not a good idea under the collector. However, if already humid air has entered the greenhouse, condensation may occur under certain conditions inside the chimney and the release of latent heat, heating the air, and increasing the buoyant force, would thus provide an additional driving force for SCPPS. Vanreken et al. [35] proposed a mathematical model for the simulation of the cloud formation process to simulate the operational characteristics of a SCPPS in southern Australia under anticipated operating conditions. The study found that for very high levels of water vapor, the use of appropriate humidification measures can produce clouds in the chimney and the formation of these cloud depends largely on the pre-assumed entrainment rate. Kashiwa et al. [36] proposed a “solar cyclone” system to achieve separation of water and air. The system has an outwardly expanding cyclone installed at the base of the chimney, where hot air flows during a sudden cooling and condensation to get water from the air. In this process, its central temperature is below the dew point. Therefore, it can produce freshwater during operation, and the whole cycle is sustainable; however, its efficiency is unclear and further research is needed.

As a matter of fact, when a small convection unit grows into a fully developed thunderstorm in the atmosphere, the entrainment in the air column adjacent to each other enters into another floating air column and will have a devastating effect on the formation of the thunderstorm cloud. The entrainment rate of the air column is inversely proportional to the radius of the cloud [37]. To enhance convection in the vertical direction and the output of air condensate, Starr and Anatii et al. [38,39] proposed to prevent entrainment by using a high chimney (chimney height of 3000 m, chimney radius of 50 m). With such a structure (which they named “aerological accelerator”), the internal ascending airflow would not be destroyed by adjacent air columns, and when the air parcel adiabatically rises in the chimney, the volume expands due to the reduced pressure. With the internal energy against external forces, the temperature will continue to decline in the process of rising, while the relative humidity of the air would be increasing. Since the water content in the air remains constant, the saturated vapor pressure decreases as the temperature decreases. When the air parcel reaches the lifting condensation level (the height at which the relative humidity of an air parcel will reach 100% when it is cooled via dry adiabatic lifting), the water vapor in the air parcel will begin to condense to form cloud droplets. Therefore, the engineering structure utilizes the spontaneous convection process in the lower atmosphere due to the unstable environmental lapse rate, and is independent of external driving. Starr calculated that water production in the wet season can reach an amount of 2000 metric tons per hour, an amount that is comparable to that of modern desalination plants; however, the cost of construction of these modern desalination plants would be around $ 1 billion [40]. Recently, Ming et al. [41,42] re-analyzed such systems to verify the “aerological accelerator” potential, and found that the system (in addition to the appropriate collection) can be used for the supply of freshwater for households and agriculture, but also allows considerable power output. Based on this, they introduced a SCPPS combination of water production and power generation.

Indeed, the atmosphere is rich in freshwater humidity. The technology of water harvesting from air, based on solar chimney presents great potential, and has an even greater practical value in dry areas. Zhou et al. [43] conducted a computer simulation of SCPP in a hot and dry desert, and found a possibility to promote the surrounding rainfall. They developed a three-dimensional mathematical model to explore the possibility of generating clouds and precipitation around the SCPP. The results showed that the relative humidity of the outlet airflow could be significantly increased due to the plume being injected into the colder environment. This may change the microclimate around the SCPP and have positive effects, such as increasing the precipitation; however, at the same time this would also increase the risk of clouding over the SCPP, thus reduced the solar radiation and the power output. Hence, taking into account the fact that the overall efficiency of the traditional SCPPS is already low, Zhou et al. [44] also compared the performance difference between the classical SCPPS and the SCPPS combined with power generation and desalination by establishing a one-dimensional compressible flow model. They found that if SCPPS was combined with power generation and seawater desalination, it would produce less power than the classic SCPPS due to the large amount of heat used for water evaporation. Moreover, in an economic analysis of the system, they found that the price of freshwater and electricity prices depend on the height of the chimney.

Motivated by the new development of SCPPS and thanks to the presence of unstable environmental lapse rate in the atmosphere, the air could cool down along the chimney and spontaneously precipitate condensed water under certain conditions. Thus, on the one hand there is the possibility for direct production of fresh water inside the solar chimney. However, as seen through the above summary of the relevant literature, there is a very important condition: the height of the chimney needs to be sufficient. This has brought numerous technical and economic problems for the practical application of solar chimney technology. On the other hand, the heating of the thermal airflow through the ground in the collector leads to a rise of the air temperature, but also reduces relative humidity. After the thermal airflow enters the chimney, it takes a long height to cool down before it reaches the dew point to precipitate the condensed water, i.e., the height of the

chimney needs to always be very high. Therefore, as previously proposed, ways are required to achieve an already high relative humidity of the thermal airflow entering into the chimney [41,42].

1.3. Research in this article

To solve the above-mentioned problems, we consider the use of both seawater and brackish water. The thermal airflow is sprayed with water and wetted by pumping or other means at the chimney entrance, so that the wet air is moved closer to the saturated state. If so, this can greatly reduce the chimney height, thus reducing the chimney construction costs and the corresponding technical problems. In this article, the desalination performance of a new device with dimensions similar to the Manzanares pilot model was numerically investigated by establishing a three-dimensional compressible flow and heat transfer mathematical model to describe the moist air, which cools down along the chimney and condenses above the lifting condensation level. The numerical model was solved in the commercial software ANSYS Fluent to obtain the pressure distributions, velocity distributions, temperature distributions, and desalination performance of the solar chimney system (SCS) under different amounts of spray droplets.

The remainder of this article is organized as follows: Section 2 introduces the mathematical model, boundary conditions, and numerical solutions based on a simplified Manzanares pilot model. Section 3 validates the reliability of the numerical procedures by comparing numerical results with experimental results. Section 4 presents the collection of numerical results. The flow performance, temperature characteristic, and the desalination performance within and without the system are analyzed. Section 5 presents an assessment of the relevant benefits and concerns for seawater desalination of the SCS. Section 6 presents the main conclusions of the numerical study and discusses future applications of this engineering structure.

2. Model description

2.1. Geometric model

When solar radiation reaches the ground through the collector and is absorbed by the ground, the ground temperature increases and the air inside the collector is heated. The air density and the relative humidity of the air are thus reduced, and the natural convection generated by the difference in air buoyancy causes a strong updraft inside the chimney. Thanks to the presence of environmental lapse rate in the atmosphere, the air can cool down along the chimney and spontaneously precipitate condensate water under certain conditions. Compared with conventional SCS, the most obvious difference is that, instead of installing the turbine, seawater droplets are sprayed at the bottom of the chimney for evaporation, and thus thermal airflow is subjected to a humidification treatment, as shown in Fig. 1(a). Therefore, this is expected to reduce chimney height and system cost to recover liquid water from the air inside the chimney by partially replicating the natural warm wet air convection process. In addition, it can be assumed that the salts, which are in the seawater droplets, fall down at the entrance of the chimney (we suppose that an electrostatic precipitator can eliminate all the different salts at 99.99%), where they are somehow removed to prevent accumulation. As a result, the idea of recovering water from the air thus became seawater desalination.

The geometric model for numerical simulation is a simplified Manzanares pilot model, as shown in Fig. 1(b). The SCS model has a chimney height of 200 m and a chimney radius of 5 m, and a circular solar collector, which covers the soil surface, has a radius of 120 m and a height of 2 m. To simulate the performance of a SCS exposed to an external environment, it has been assumed that the model is placed in a virtually non-existent cube with dimensions in the x, y, z directions of 600 m, 400 m, and 300 m, respectively. Each surface of the cube is set to a different boundary condition, which will be described in detail below. At the velocity inlet boundary, the X-axis is parallel to the velocity direction of the ambient crosswind, and the Z-axis is perpendicular to the velocity direction. Assuming that the surface perpendicular to the Y axis has a symmetrical characteristic, the geometric model can be simplified, taking only half of the system model, as shown in Fig. 1(b). Thus, after simplification, the geometric dimensions of the entire cube were 600 m, 200 m, and 300 m in the x, y, z directions, respectively. This assumption was acceptable in stable numerical calculations. At the same time, the influence of the thermal storage layer was not considered and therefore was not added to the calculation model. This is because, if both the external environment and the four parts of the SCS are considered: collector, turbine, chimney, and the thermal storage layer, the number of calculated grids will exceed the computational power of the available computer, thus leading to complicated and time-consuming calculation.

2.2. Mathematical model

For solar chimney systems, it is generally considered that the flow within the system is a natural convection caused by solar radiation, heating the ground under the greenhouse. The number of natural convection intensity criteria that are measured by the buoyancy force is the Rayleigh number, which is defined as follows:

$$Ra = \frac{g\beta\Delta T L^3}{av} \tag{1}$$

where g represents the gravitational acceleration; β represents the coefficient of thermal expansion; ΔT represents the maximum

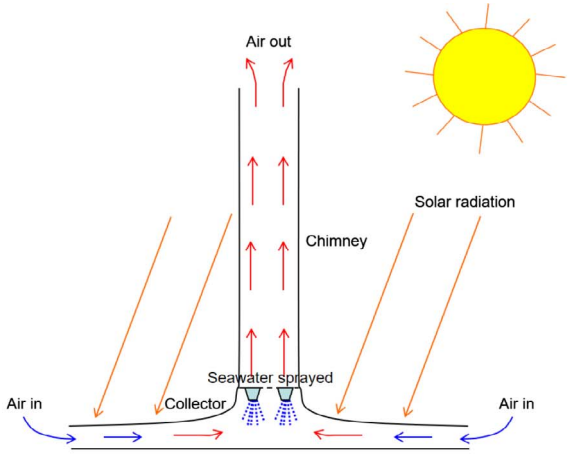

(a) Sketch of the Seawater Desalination Mechanism of the Solar Chimney System

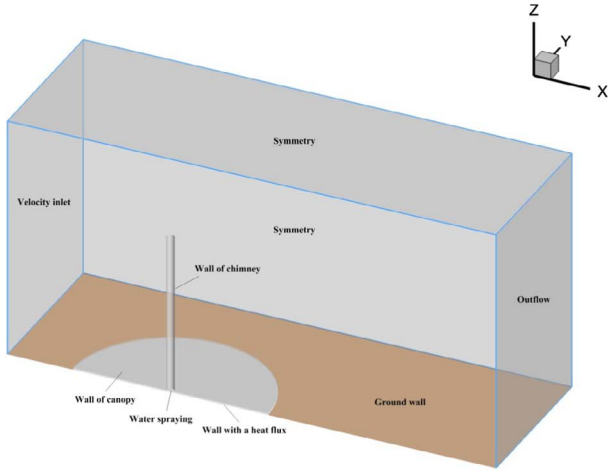

(b) Three-Dimensional Geometric Model of the Solar Chimney System

Fig. 1. Geometric model of the solar Chimney system for seawater desalination.

temperature increment within the system; L represents the height of the collector; and α represents the thermal diffusion coefficient; ν indicates the kinematic viscosity. After preliminary calculation, it was found that the Rayleigh number was higher than 10^{10}, i.e., it is necessary to select the appropriate turbulence mathematical model to describe the fluid flow in the solar chimney system, which exceeds the upper limit of the natural convection from the laminar flow to the turbulence. In general, due to the existence of three-dimensional turbines in the traditional SCS, the system will produce complex a strong vortex and turbulence, and theoretically, using a RNG or Realizable model will be more accurate. However, in this article, due to the consideration of the SCS in the performance of desalination, the turbine for power generation units was not considered. Therefore, a more economical standard $k-\varepsilon$ turbulence model was adopted, and the stability of this model enabled low computational cost. The density of air in the system was mainly caused by changes in temperature rather than pressure changes. Thus, the air density was defined by the UDF to assume that the airflow within the system was a compressible flow, and the ideal gas law was used to represent the relationship between the density and temperature of the natural convection.

The atmospheric pressure and atmospheric density can be calculated by the following formula [16]:

$$p_\infty(z) = p_\infty(0)\left(1-\frac{\kappa-1}{\kappa}\frac{z}{H_0}\right)^{\kappa/(\kappa-1)} \tag{2}$$

$$\rho_\infty(z) = \rho_\infty(0)\left(1-\frac{\kappa-1}{\kappa}\frac{z}{H_0}\right)^{1/(\kappa-1)} \tag{3}$$

where p_∞ represents the atmospheric pressure; ρ_∞ represents the ambient air density; z represents the height from the ground; R_g represents the ideal gas constant, with a value of 287.05 J/(kg K); g represents the acceleration of gravity, with a value of 9.8 m/s^2; κ represents the specific heat ratio, with a value of 1.235 for the standard atmospheric; H_0 represents the atmospheric scale height, $H_0 = \frac{R_g T_\infty(0)}{g}$.

The relative humidity RH is the ratio of the partial pressure of the water vapor in the air to the saturated pressure of the water vapor at a certain temperature:

$$RH = \frac{p_v}{p_S} \tag{4}$$

The saturated pressure of the water vapor can be calculated with the following equation [45]:

$$\ln\left(\frac{p_S}{p_C}\right) = \left(\frac{T_C}{T}-1\right)\times\sum_{i=1}^{8} F_i[a(T-T_P)]^{i-1} \tag{5}$$

where

$p_C = 22.089$ MPa; $T_C = 647.286$ K;
$F_1 = -7.4192420$; $F_2 = 2.9721000\times10^{-1}$;
$F_3 = -1.1552860\times10^{-1}$; $F_4 = 8.6856350\times10^{-3}$;
$F_5 = 1.0940980\times10^{-3}$; $F_6 = -4.3999300\times10^{-3}$;
$F_7 = 2.5206580\times10^{-3}$; $F_8 = -5.2186840\times10^{-4}$.
$a = 0.01$; $T_P = 338.15$ K.

Continuity equation:

$$\frac{\partial\rho}{\partial t} + \frac{\partial}{\partial x_i}(\rho u_i) = S_m \tag{6}$$

Wherein the mass source term S_m was added to the continuous phase or removed from the continuous phase dependent on the evaporation or condensation of the droplets.

When the relative humidity RH ≤ 1,

$$S_m = 0 \tag{7}$$

When the relative humidity RH > 1,

$$S_m = -coeff\cdot\frac{p_v-p_S}{R_s T}\cdot u_j \tag{8}$$

where *coeff* represents the condensation coefficient, which indicates the probability that a vapor molecule escapes or absorbs from the interface. This probability value generally needs to be matched with the experimental data, which is influenced by the temperature during the temperature-driven mass transfer. In this study, *coeff* was chosen as the suggested value in the ANSYS Fluent, i.e., *coeff* = 0.1. R_s represents the gas constant of the water vapor, and R_s = 461 J/(kg K).

The air density can be calculated from the equation of state:

$$\rho = \frac{p_\infty-p_v}{R_g T} + \frac{p_v}{R_s T} \tag{9}$$

Navier-Stokes equation:

$$\frac{\partial}{\partial t}(\rho u_i) + \frac{\partial}{\partial x_j}(\rho u_i u_j) = -\frac{\partial p}{\partial x_i} + \frac{\partial\tau_{ij}}{\partial x_j} + \rho g_i + S_F \tag{10}$$

where the stress tensor τ_{ij} was defined as:

$$\tau_{ij} = \left[\mu\left(\frac{\partial u_i}{\partial x_j} + \frac{\partial u_j}{\partial x_i}\right)\right] - \frac{2}{3}\mu\frac{\partial u_i}{\partial x_i}\delta_{ij} \tag{11}$$

The momentum source term S_F was defined as:

$$S_F = (\rho-\rho_\infty)g \tag{12}$$

Energy equation:

$$\frac{\partial}{\partial t}(\rho E) + \frac{\partial}{\partial x_i}(u_i(\rho E + p)) = \frac{\partial}{\partial x_j}\left(k_{eff}\frac{\partial T}{\partial x_j} - \sum_j h_j J_j + u_j(\tau_{ij})_{eff}\right) + S_h \tag{13}$$

where k_{eff} represents the effective thermal conductivity ($k + k_t$, k_t represents turbulent thermal conductivity); J_j represents the diffusion flux of the component j; S_h includes chemical reaction or any other volume heat source, and with an air relative humidity of RH ≤ 1,

$$S_h = -\rho g u_j \tag{14}$$

where the energy source term S_h indicates the enthalpy loss when the internal air of the chimney was converted to the gravity potential, and when the relative humidity RH > 1,

$$S_h = \left(\frac{p_v-p_S}{R_S T}\right)\gamma\cdot coeff - \rho g u_j \tag{15}$$

where γ represents the latent heat released from the condensation of water vapor, and γ = 2257000 J/kg.$(\tau_{ij})_{eff}$ represents the deviatoric stress tensor, which was defined as:

$$(\tau_{ij})_{eff} = \mu_{eff}\left(\frac{\partial u_j}{\partial x_i} + \frac{\partial u_i}{\partial x_j}\right) - \frac{2}{3}\mu_{eff}\frac{\partial u_k}{\partial x_k}\delta_{ij} \tag{16}$$

In Eq. (13),

$$E = h - \frac{p}{\rho} + \frac{v^2}{2} \tag{17}$$

where the sensible enthalpy h was defined as:

$$h = \sum_j Y_j h_j + \frac{p}{\rho} \tag{18}$$

where Y_j represents the mass fraction of component j.

Turbulent kinetic energy k equation:

$$\frac{\partial}{\partial t}(\rho k) + \frac{\partial}{\partial x_i}(\rho k u_i) = \frac{\partial}{\partial x_j}\left[\left(\mu + \frac{\mu_t}{\sigma_k}\right)\frac{\partial k}{\partial x_j}\right] + G_k + G_b - \rho\varepsilon - Y_M + S_k \tag{19}$$

Turbulence dissipation ε equation:

$$\frac{\partial}{\partial t}(\rho\varepsilon) + \frac{\partial}{\partial x_i}(\rho\varepsilon u_i) = \frac{\partial}{\partial x_j}\left[\left(\mu + \frac{\mu_t}{\sigma_\varepsilon}\right)\frac{\partial \varepsilon}{\partial x_j}\right] + C_{1\varepsilon}\frac{\varepsilon}{k}(G_k + C_{3\varepsilon}G_b) - C_{2\varepsilon}\rho\frac{\varepsilon^2}{k} + S_\varepsilon \quad (20)$$

where G_k represents the turbulent kinetic energy due to the average velocity gradient, which can be defined as: $G_k = -\rho\overline{u_i' u_j'}(\partial u_j/\partial x_i)$; G_b represents the turbulent kinetic energy due to buoyancy; σ_k and σ_ε are the turbulence Prandtl number: $\sigma_k = 1.0$, $\sigma_\varepsilon = 1.3$. $C_{1\varepsilon}$ and $C_{2\varepsilon}$ represent constants: $C_{1\varepsilon} = 1.44$, $C_{2\varepsilon} = 1.92$. $\mu_t = (C_\mu \rho k^2/\varepsilon)$, and $C_\mu = 0.09$.

Species transport equation:

$$\frac{\partial \rho Y_{H_2O}}{\partial t} + \frac{\partial}{\partial x_j}(\rho Y_{H_2O} u_i) = \frac{\partial}{\partial x_j}\left[\left(\rho D_{H_2O} + \frac{\mu_t}{Sc_t}\right)\frac{\partial Y_{H_2O}}{\partial x_j}\right] + S_{H_2O} \quad (21)$$

where S_{H_2O} represents the addition or removal of water vapor within the air due to evaporation or condensation, respectively.

Scalar equation:

$$\frac{\partial}{\partial t}(\rho\phi) + \frac{\partial}{\partial x_j}(\rho\phi u_i) = \frac{\partial}{\partial x_j}\left(\Gamma\frac{\partial \phi}{\partial x_j}\right) + S_\phi \quad (22)$$

where ϕ represents any scalar, and Γ represents the diffusion coefficient.

2.3. Boundary conditions

For the SCS considering the external environment, to obtain accurate results, the boundary conditions and environmental parameters had to be carefully considered. The geometric model in Fig. 1 has presented some boundary conditions and the corresponding coordinate system. The detailed boundary conditions are listed in Table 1.

For the calculation, it was assumed that the flow of the ambient crosswind has reached full development and that the ambient air temperature remained constant at 293 K and the relative humidity was 82% before flowing into the system. According to the logarithmic law of the wind profile of the atmospheric boundary layer proposed by Prandtl in 1932, the ambient crosswind speed can be fitted into the following formula [46]:

$$v = w = 0 \quad (23)$$

$$u = 1/\kappa(\tau_S/\rho)^{1/2}\ln(z/z_0) \quad (24)$$

where τ_S represents the ground shear stress and z_0 represents the aerodynamic roughness of the ground. In the calculation, the ground was assumed to be a flat desert, and therefore, κ was set as 0.4 and z_0 was set as 0.01 m. Then, τ_S could be calculated according to the wind speed at a reference height, which was the height of the chimney in this article, and the wind speed at the chimney height was assumed to be $U_{200} = 5$ m/s. In this case, this is able to simulate the chimney outlet airflow under the ambient wind, while at the same time, it also assumes a negligible role of ambient wind to not weaken the system flow performance to much [14].

The relative static pressure represents the static pressure difference between the system and the same height ambient and can be used to simulate the entire pressure distribution of the system, which has been verified by Pastohr et al. [47], Ming et al. [15], and Sangi et al. [48]. The ground below collector and outer area are included in the ground boundary conditions. The outer area ground was assumed to be in an isothermal wall boundary condition with a temperature of 318 K. This assumption may more or less impact the accuracy of the simulation results than the actual operating conditions of the solar chimney system; however, it will not have a significant impact on the study of the seawater desalination application of the solar chimney system. The radiant heat transfer between the collector and other walls is not taken into account. Furthermore, the solar radiation was assumed uniform with a vertical incident, while the ground was uniform and isotropic. Therefore, the calculated solar radiation was set to 857 W/m^2, and the corresponding heat flux on the ground was set to 600 W/m^2 due to heat loss and heat transfer energy loss [14].

2.4. Meshing skills

Fig. 2 shows the grid distribution of the geometric model. The hexahedron (HEX) meshing method used in the model was effective due to its economy and it can effectively reduce false diffusion. In Fig. 2(a), the velocity gradient and the temperature gradient near the wall of the chimney are both relatively large; therefore, the fine grid was used to simulate the flow inside the chimney. Fig. 2(b) shows the grid distribution of the local area within and without the chimney. To reduce the number of grids and to improve the accuracy of the calculation, a finer boundary layer grid was used in the chimney wall, the wall of the collector wall, and the ground wall. At the same time, the turbulence at the connection between the collector and the chimney was strong; therefore, the use of structured mesh enabled to reduce the error caused by the complex flow.

2.5. Numerical method

The mathematical model was solved with the finite volume method in the commercial software ANSYS Fluent. The pressure-velocity coupling used the SIMPLE algorithm. The convective term chose the QUICK scheme to discrete, and the spatial discrete method of the diffusive terms adopted the second order upwind scheme. Furthermore, due to the existence of different length scales in the model, the double-precision solver was chosen. To monitor the convergence of the equations, the convergence criterion of the energy equation was set to 10^{-8}, and the convergence criterion of the remaining equations was set to 10^{-6}. The iteration was calculated until the relative error of each variable was lower than the convergence criterion, and the result no longer changed.

To verify the grid independence of the numerical simulation results, under the same environmental conditions and operating conditions (solar radiation is 857 W/m^2, amount of spray droplets of 0), three calculation cases were verified with the number of grids of 2,205,900, 3,335,450, and 4,037,650, respectively. The results are shown in Fig. 3. The simulation results showed that the volume flow rate of the chimney outlet was 256.5 m^3/s, 250.5 m^3/s, and 248.6 m^3/s, while the average temperature of the chimney outlet was 302.09 K, 301.14 K, and 301.12 K, respectively. From a comparison of the results, it was found that there were only about 2% deviation among these three calculation cases, indicating that the numerical results used in the model are independent of the grid, and the impact for increasing or decreasing the grid on the calculation result was small. Therefore, to minimize the calculation error and to reduce the computational cost, in this article we chose the number of grid as 3,335,450 to perform the numerical analysis.

Table 1
Boundary conditions.

Place	Boundary type	Value
x = 0 m	Velocity inlet	$u = 1/\kappa(\tau_S/\rho)^{1/2}\ln(z/z_0)$ $U_{200} = 5$ m/s, $T = 293$ K, $RH = 82\%$
x = 600 m	Outflow	
y = 0 m	Symmetry	
y = 200 m	Symmetry	
z = 300 m	Symmetry	
Ground under the canopy	No-slip wall	600 W/m^2
Ground outside the collector	No-slip wall	318 K
Surface of the chimney	No-slip wall	$q = 0$ W/m^2
Chimney surface	No-slip wall	$q = 0$ W/m^2

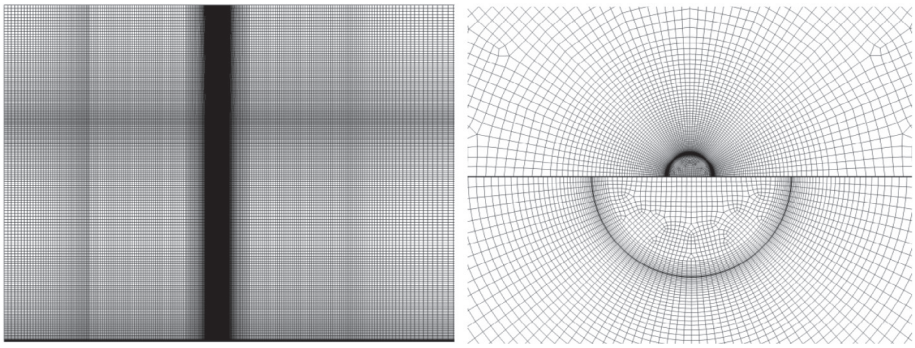

(a) y=0 plane (b) Chimney-collector local area

Fig. 2. Grid distributions: (a) y = 0 plane; (b) Chimney-collector local area.

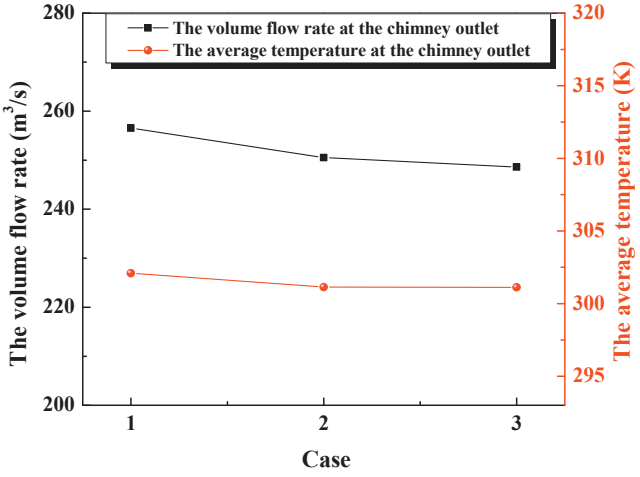

Fig. 3. Grid-independent validation.

3. Validation

To verify the reliability of the numerical procedures, the simulated chimney inlet air temperature was compared to experimental results collected on 2nd September 1982 of the Spanish prototype. The ambient conditions and operation conditions were set according to literature [2]. Moreover, the turbine was regarded as a reverse fan with pressure drop at the exit of the collector, which was identical to the one used by Xu et al. [49] and Ming et al. [15]. Fig. 4 shows that the simulation results in this article were quite consistent with the experimental results, as it shows a maximal temperature difference below 2 K. The disparity between them could be attributed to several reasons such as the heat dissipation from the system to the ambience, flow and heat transfer resistance of the system, and ignoring the role of the energy storage layer; however, the overall difference was acceptable. Hence, it can be concluded that the numerical codes and procedures applied in this paper were feasible to some extent.

It is worth noting that the SCS studied in this paper was different from the conventional SCPPS. Instead of installing the turbine, water droplets were sprayed for evaporation at the bottom of the chimney. Thus, we were more concerned about the desalination performance of this plant variant. However, with the change of operation conditions, the thermo-fluidmechanical process inside the system was completely different from that of the conventional system. It is difficult to find appropriate data in the existing experimental and computational results, which has posed problems for the validation process. Therefore, the experimentation of this small plant variant was also one of the main research directions for the future.

4. Results and analysis

The seawater droplets were uniformly sprayed in the form of a surface using an artificial device when the airflow passed through the bottom of the chimney. The diameter of the spray droplets was 30×10^{-6} m and the droplet temperature was retained at the same temperature than the airflow at the bottom of the chimney. As the air inside the collector was heated by the solar radiation, the relative humidity was low. It was assumed that once the droplets were injected when the airflow entered the chimney, evaporation occurred, so that the relative humidity of the airflow increased. To analyze the effectiveness of seawater desalination performance of the solar chimney system, the flow and heat transfer characteristics of the system were studied, respectively. In the flow characteristics, the driving force of the system could be attributed to the relative static pressure change in the cause of natural convection, but also to a measure of flow strength of the key factors. Airflow velocity was a direct reflection of the flow of speed, and can visually show the impact of spray on the flow of the system. Then, the temperature characteristics of the system also played a vital role in natural convection. Considering the parameters of the performance of seawater desalination, the change of air relative humidity, the change of water content, and the change of condensed water in the different amount of spray droplets needs to be examined.

4.1. Comparisons of flow performance

Fig. 5 shows the relative static pressure distributions of the SCS under different mass flow rate of spray droplets. Fig. 5 shows that the

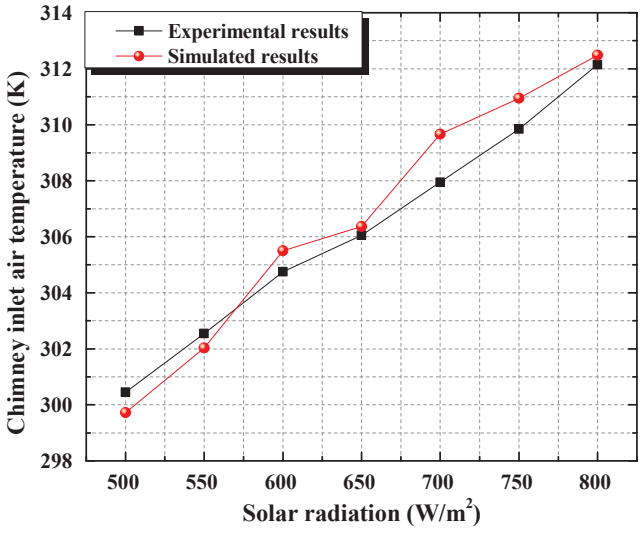

Fig. 4. Comparison between simulation results and experimental results.

relative static pressure of the external environment of the system decreases with increasing altitude, and the distribution level was relatively clear: the environment was basically in a stable state. The setting of the SCS, on the one hand plays the role of blocking the flow of the environment and results in a change of the relative static pressure field of the local environment. On the other hand, the relative static pressure inside the chimney increases with height. Moreover, it can be found that at the bottom of the chimney an area exists with relatively high static pressure, which is a stagnation zone. In general, the stagnation zone was generated at the local zone due to the chimney effect, and the region's air velocity was very small, while the airflow temperature was higher. A relatively small static pressure value could be observed above the stagnant zone. In fact, the driving force of the chimney system was caused by the pressure difference between the ambient pressure and the internal pressure of the system, which could drive the thermal airflow to rise up the chimney, and the minimum static pressure can sometimes reflect the flow strength. Due to the effect of ambient crosswinds, the stagnation zone appeared on the right side of the bottom of the chimney, while the minimum static pressure appeared at the left side of the bottom of the chimney and decreased with increasing amount of spray droplets. Overall, the pressure difference between the surroundings and the system decreased with the increasing amount of spray droplets. This was because the latent heat of evaporation of the spray droplets consumed the heat of the thermal airflow, resulting in a decrease in the driving force in the system, and a weakening of the natural convection, as shown in Fig. 5(a)–(c), the corresponding amounts of spray droplets were 0 kg/s, 0.1 kg/s, and 0.3 kg/s, respectively. Furthermore, the condensation phase transformation did not occur by monitoring the airflow at the exit of the chimney.

In Fig. 5(d), the corresponding amount of spray droplets was 0.5 kg/s, and it was found that the condensation phase transformation occurred inside the chimney. Fig. 5(d) showed that the relative static pressure difference of the SCS and the ambient changed relatively fast. The relative static pressure of the ambient was still decreasing with increasing altitude, at a more obvious distribution level. The relative static pressure distribution inside the chimney was obviously different from that of the first three graphs with smaller amounts of spray droplets. The relative static pressure decreased with increasing chimney height, and the position of the stagnation zone at the bottom of the chimney was towards the right, the relative static pressure distribution inside the collector had also changed. In general, when the amount of spray droplets increased to a phase change that caused the airflow inside the chimney to undergo condensation, the difference between the ambient and the SCS decreased, which may cause a weakening of the air flow within the system. At the same time, the relative static pressure of the entire system will change.

Fig. 6 shows the distribution curve of the relative static pressure along the chimney height with different amounts of spray droplets. When the amounts of spray droplets were 0 kg/s, 0.1 kg/s, 0.3 kg/s, and 0.4 kg/s, the relative static pressure at the bottom of the chimney had a minimum. With increasing amount of spray droplets, it can be clearly seen that the minimum static pressure increased, i.e., the spray droplets once injected and completely evaporated will affect the flow within the system. Along the height of the chimney, the relative static pressure continued to increase until near the chimney exit (about 210 m height in the figure). Then, under the effect of the ambient crosswind, the relative static pressure maintained consistent with the ambient pressure. The relative static pressure values in the case of these four amounts of spray droplets were combined into a curve and did not change as the height increased.

When the amount of spray droplets was 0.5 kg/s, it was clear that the original minimum static pressure of the relative static pressure curve disappeared. The relative static pressure after passing through the bottom of the chimney was still decreasing with increasing height; however, the magnitude of the reduction did not begin to be so intense at the bottom of the chimney. Moreover, at the farther exit of the

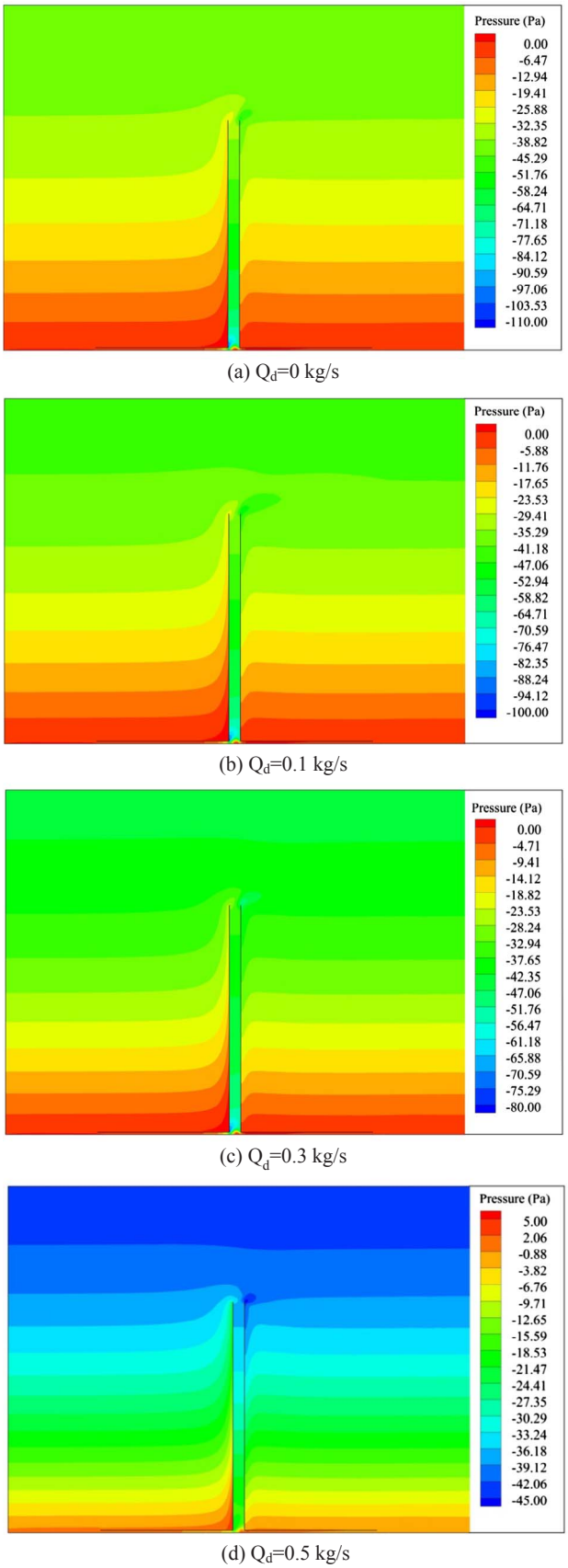

Fig. 5. Relative static pressure distributions under different mass flow rates of spray droplets.

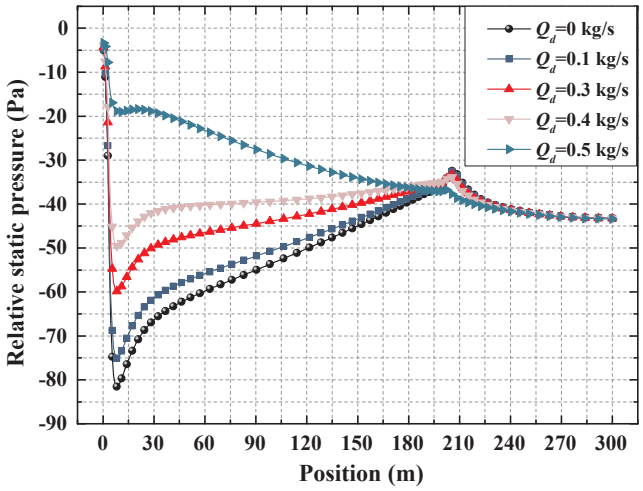

Fig. 6. Relative static pressure distribution curves in the height direction of the chimney.

chimney (about 225 m in the figure), the curve converged with the preceding four curves, i.e., the relative static pressure was consistent with the environment.

Generally, when the amount of spray droplets increased, the relative static pressure distribution inside the chimney was noticeably affected, and the relative static pressure difference between the inside and the outside of the system decreased, which will weaken the flow intensity in the system. The reason for this phenomenon is that, the increase in the amount of spray will cause the vapor to absorb more latent heat of vaporization during the evaporation process and thus reduce the air temperature in the system. When the amount of spray droplets increased to the point where a condensation phase change occurred inside the chimney, the relative static pressure distribution will change greatly, which may lead to a deterioration in the flow performance of the system. Therefore, it is necessary to further analyze the flow performance in the system under different amounts of spray droplets.

Fig. 7 shows the average air velocity distributions of the SCS under different mass flow rates of spray droplets. When the inflowing wind approached the solar chimney, a strong elevated trailing vortex system was generated, and flow separation and strong turbulence exist near the top of the chimney. Thus, the flow field in the ambient was disturbed by the blockage of the chimney. The average air velocity leeward of the chimney was very low, in which a “shadow area” formed. However, because the diameter of the chimney was also relatively small, the “shadow area” on the ambient flow field could be neglected. The air near the collector flowed towards the center of the collector under the stack effect, while at the same time, it was heated by the ground so that the air temperature gradually increased. Due to the effect of the ambient crosswind, the velocity distributions in the collector showed that the wind speed of the windward side was large, while that of the leeward side was smaller. The heated air was sucked into the chimney, and the updraft reached the peak value of the velocity at the bottom of the chimney; then, it steadily rose along the chimney and eventually flowed out. As can be seen from Fig. 7, under the effect of ambient crosswind, the velocity peak area (red area) at the bottom of the chimney was significantly tilted to the right, while the left side of the airflow rate was relatively low. Therefore, the ambient crosswind will have a greater impact on the airflow within the solar system.

When the amounts of spray droplets were 0 kg/s, 0.1 kg/s, and 0.3 kg/s, respectively, the average velocity distributions of air across the system and the ambient were almost identical. The only difference was that with increasing amount of spray droplets, the maximum velocity of air in the system was slightly reduced, reflecting that the increase in the amount of spray droplets weakened the air flow within the

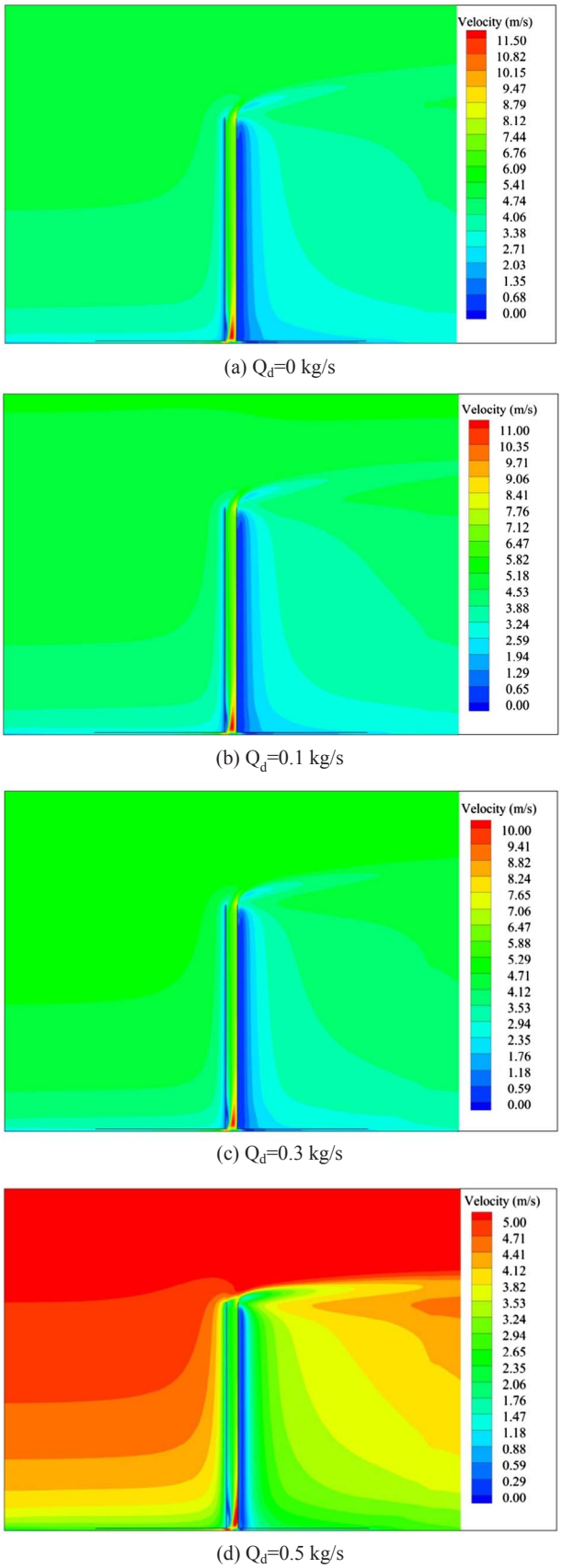

Fig. 7. Air velocity distributions under different mass flow rates of spray droplets.

system, but the magnitude of the weakening was low. However, when the amount of spray droplets was 0.5 kg/s, a condensation phase transformation occurred inside the chimney, significantly weakening the flow within the system. The velocity peak area (read area) was still observed near the bottom of the chimney, but the air speed was closer to the ambient wind speed.

To quantitatively analyze the air velocity in the chimney, Fig. 8 shows the average air velocity profiles of the updraft along the chimney. When the amounts of spray droplets were 0 kg/s, 0.1 kg/s, and 0.3 kg/s, the average air velocity profiles along the chimney were similar: the airflow reached a peak velocity at the bottom of the chimney, and then a sharp drop in the height of about 60 m was observed; after that, the velocity tended to be stable and the airflow steadily increased inside the chimney. At the exit of the chimney, the velocity of the airflow dropped sharply and four curves reached the lowest velocity at the same height (near 210 m in the figure). The difference between the four velocity profiles was: with the increasing amount of spray droplets, the velocity curve was declining because the flow performance of the system weakened; however, the magnitude of the weakening was relatively small. However, when the amount of spray droplets was 0.5 kg/s, it was found that the velocity curve was reduced greatly. The average air velocity will still reach the peak speed at the bottom of the chimney, but compared to the first four cases, the peak speed was much smaller. After the updraft tended to be stable in the chimney, the value of the velocity was low with only about 2.5 m/s. Then the air velocity began to sharply increase near the exit of the chimney, and eventually rose until the ambient wind speed, with the first four curves together into the same curve. Therefore, when the bottom of the chimney was sprayed for humidification treatment, and if the updraft inside the chimney was not condensed, the increase in the amount of spray droplets would gradually weaken the flow performance within the system; however, the magnitude of the weakening was not significant. However, when the amount of spray droplets reached the condensation phase transition, it occurred inside the chimney and the flow within the chimney was comparatively weak. The reason may be that the amount of dissipated heat when the spray droplets evaporated was much higher than the heat released during air condensation. Therefore, the air temperature sharply reduced and the driving force of the SCS weakened, thus causing the flow within the system to weaken.

4.2. Comparisons of temperature characteristics

To further analyze the cause of the deterioration of the flow performance of the SCS after spraying, Fig. 9 shows average air temperature distributions of SCSs under different mass flow rates of spray droplets. When the ground absorbed solar radiation and heated the air inside the collector, the air temperature inside the system increased, thus the air density was below that of the ambient, and an updraft was generated in the chimney. The air near the collector gradually flowed to the center under the stack effect, and the air temperature at the leeward side of the collector was higher due the effect of ambient crosswind, as shown in Fig. 9. When warmed air flowed to the center of the collector, the air temperature was very high. Then, the warmed air flowed up the chimney via the buoyant force, and the air temperature decreased with increasing chimney height. However, since in this study the height of the chimney was low, the temperature change of the airflow was not significant. As the updraft passed through the exit of the chimney, it rapidly converged with the ambient crosswind, and the temperature of the updraft was gradually reduced to ambient temperature not far from the chimney outlet. In summary, when the amounts of spray droplets were 0 kg/s, 0.1 kg/s, and 0.3 kg/s, the temperature change of the updraft inside the chimney was not obvious. When the amount of spray droplets was 0.5 kg/s, the average temperature of the updraft rapidly decreased as it passed through the bottom of the chimney (where the spray droplets were injected) and reached a much closer value that the ambient air temperature. The temperature drop of the air in the chimney and the high relative humidity affected the condensation of the air in the chimney.

As a consequence, if the air inside the chimney was to be condensed, the air temperature after the spray would be low enough to reach the dew point; however, this would reduce the temperature difference between the system and the ambient, thus weakening the flow performance of the system.

To investigate the effect of different amounts of spray droplets on the temperature distributions of updraft along the chimney, Fig. 10 shows the average air temperature profiles of updraft in the height direction of the chimney. The ground absorbs solar radiation and heats the air inside the collector; consequently, the air temperature near the ground was maximal at about 309 K. At a very short distance from the bottom of the chimney, the temperature of the updraft was rapidly reduced because the updraft had passed through the stagnant zone, in which the air temperature was higher and air velocity was lower. Afterwards, the updraft steadily increased in the chimney, and the air temperature slowly decreased as the chimney height increases. At last, not far from the chimney exit, the air temperature rapidly dropped to ambient temperature. In general, the air temperature profiles of the updraft in the chimney were generally consistent with the amount of spray droplets, and as the amount of spray increased, it became clear that the air temperature profile decreased. In other words, more heat was utilized by the evaporation of spray droplets, resulting in the fact that air temperature continued to decrease. When the amount of spray droplets reached 0.5 kg/s, the air temperature reached the dew point inside the chimney, and a condensation phase transformation occurred during the air ascending process. However, the condensed latent heat seemed insufficient to compensate for the heat of the evaporation of spray droplets and consequently, the temperature curve was very low.

In summary, when the thermal airflow was sprayed and humidified, the air temperature was inevitably reduced, and only the airflow reached the dew point during the rise inside the chimney, the condensing phase transformation was able to occur and precipitate freshwater at this time. This reduced the temperature difference between the system and the ambient, resulting in deterioration of the flow performance of the SCS. The reduction of air temperature will be a prerequisite for the desalination of solar chimneys. Thus, more detailed studies are required on the desalination performance of the SCS.

4.3. Comparisons of desalination performance

The above analysis shows that with the increasing amount of spray droplets, the flow and temperature characteristics of the SCS changed

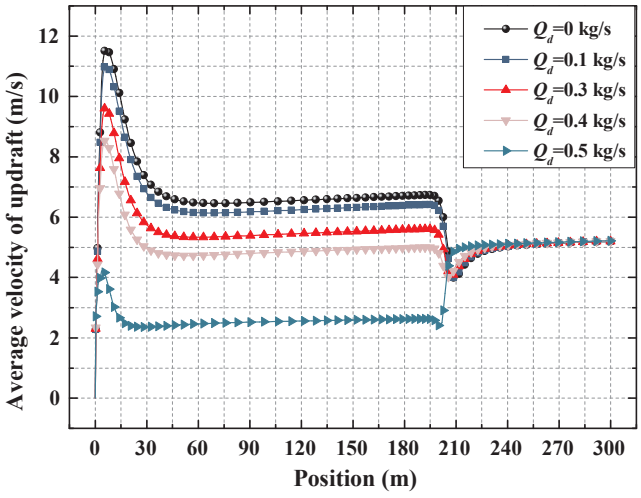

Fig. 8. Air velocity curves in the height direction of the chimney.

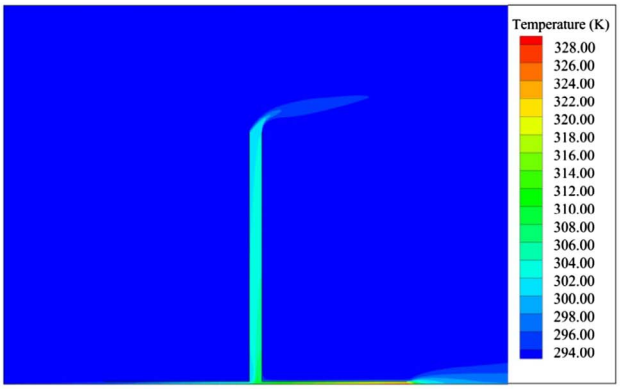

(a) Q_d=0 kg/s

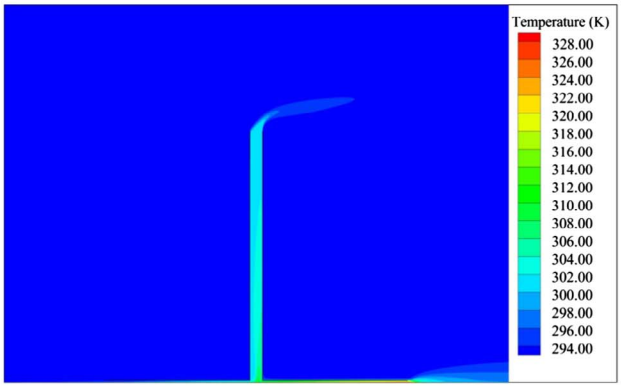

(b) Q_d=0.1 kg/s

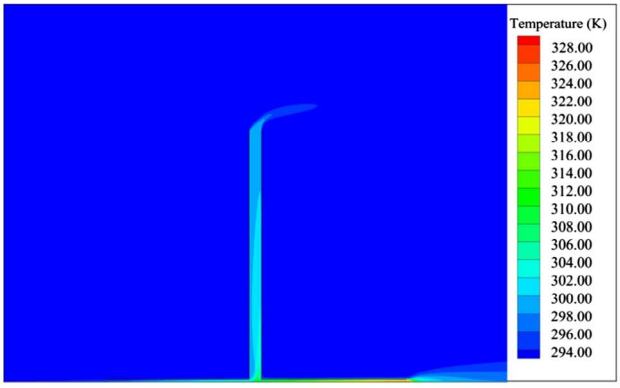

(c) Q_d=0.3 kg/s

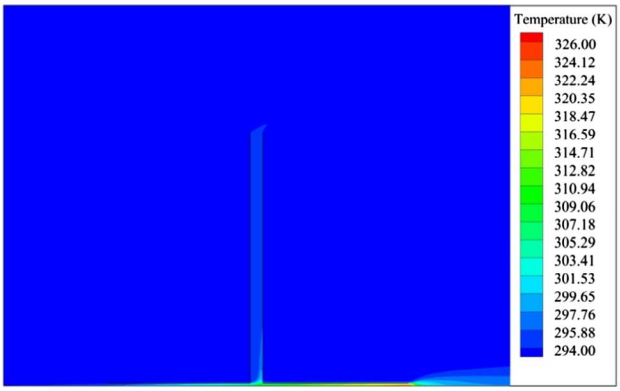

(d) Q_d=0.5 kg/s

Fig. 9. Air temperature distributions under different mass flow rates of spray droplets.

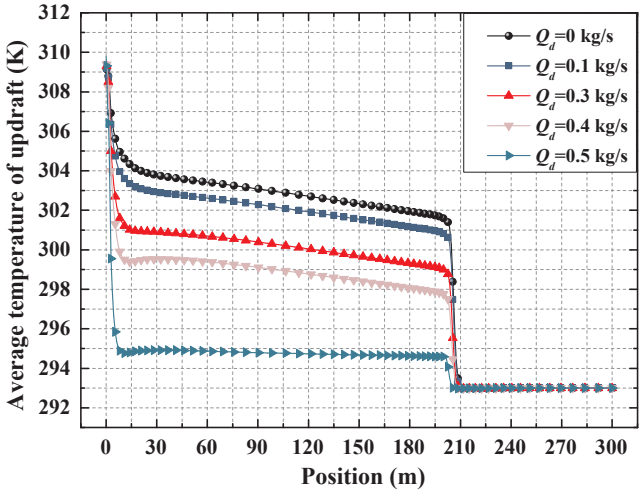

Fig. 10. Air temperature curves in the height direction of the chimney.

significantly, lowering the air temperature, and decreasing the flow rate. Thus, the weakening of the flow performance of the system caused a reduction of airflow rate, which was very unfavorable for the traditional SCS power generation performance. Therefore, the reader may pose the question of whether the effects of the flow and temperature characteristics on the desalination performance of the SCS were favorable or unfavorable.

Fig. 11 shows the mass fraction distributions of moisture in the air under different mass flow rates of spray droplets. Fig. 11 shows that with the evaporation of spray droplets at the bottom of the chimney, the moisture content of the air also changed. When the amount of sprayed water was insufficient to cause the condensation of the air inside the chimney during the ascending process, the air moisture content at the inlet of the chimney was significantly higher and the “evaporation zone” appeared at the bottom of the chimney, where the moisture had completely evaporated within this zone. After the spray droplets had evaporated completely, the resulting humidity rose and cooled down along the chimney via the buoyancy force, and the moisture content of the air remained constant during this process. When the updraft flowed through the chimney exit and into the ambient, due to the mixing of dry air in the vicinity, the moisture content of updraft flow was consistent with that of the ambient at a distance not far from the chimney outlet, as shown in Fig. 11(a). When the amount of spray droplets was 0.3 kg/s, the moist air flowed along the ambient crosswind with a certain degree of curvature after flowing out of the chimney, and the moisture content of air in the flow area was significantly higher than that of the ambient. Therefore, this process on the one hand made it possible to change the local environment of the microclimate. On the other hand, the increase of the moisture content of air also contributed to the enhancement of precipitation in the local area around the system, as shown in Fig. 11(b). Moreover, it can be found that when the amount of spray droplets was 0.5 kg/s, the moisture content of the air inside the chimney was significantly higher than in the first two cases, and the curvature of the outflow in the environment was lower than that of the first two cases. The increase of the amount of spray droplets increased in the moisture content in the air, and the air density increased as temperature was lowered. However, the increase in the amount of spray droplets also caused the flow inside the chimney to weaken and the flow rate of updraft was thus reduced; therefore, the chimney outflow was lower than that of the first two cases with lower amounts of spray droplets. However, from another point of view, it may be more conducive to improve the local microclimate and to increase the

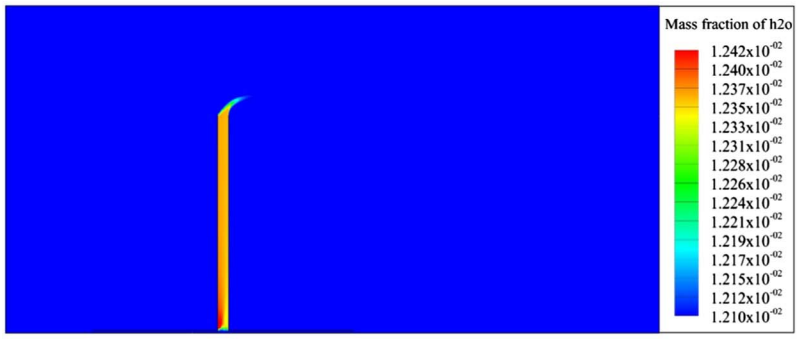

(a) Q_d=0.1 kg/s

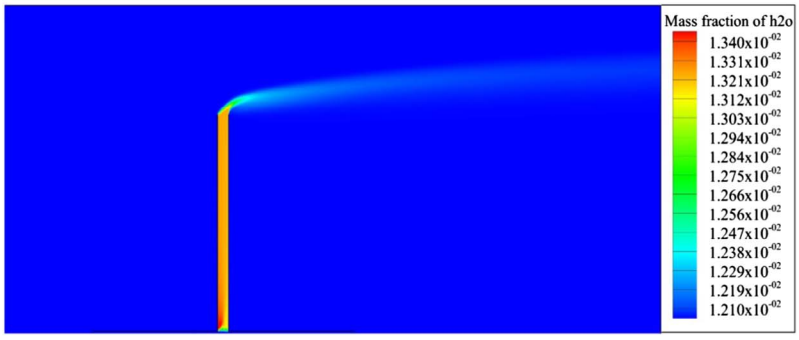

(b) Q_d=0.3 kg/s

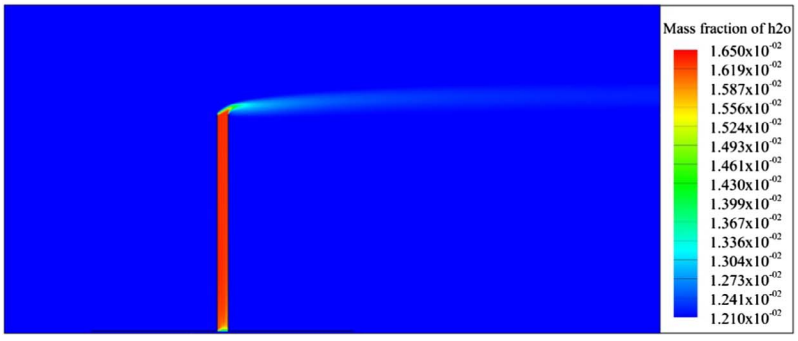

(c) Q_d=0.5 kg/s

Fig. 11. Mass fraction of moisture in the air distributions under different mass flow rates of spray droplets.

precipitation of the local area, thus this needs to be verified in a future study.

Fig. 12 shows the three-dimensional iso-surface distributions of the moisture content of air in the SCS under different mass flow rates of spray droplets. With the increase of the amount of sprayed liquid droplets, the flow pattern of the chimney outflow showed an inconsistent distribution in the environment. Furthermore, the flow distance of the chimney outflow was farther and the air moisture content in the flow area was higher. The above analysis showed that the flow in the chimney was weakened when the amount of spray droplets increased. Therefore, it can be concluded that the influence of air moisture content of chimney outflow on the environment was that the effect on the microclimate of the local environment did not decrease with the decrease of the flow intensity in the system, but rather increased with the increase of the amount of spray droplets. This was because the increase in the internal flow of the chimney facilitated the updraft in the chimney to reach a higher height after the flow passed through the exit of the chimney, i.e., higher curvature of the outflow. The outflow to the nearby local area environment was determined by the ambient crosswind; therefore, when the ambient crosswind conditions were constant, a higher amount of spray droplets will increase the moisture content in the air and have a greater impact on the local environment. However, increasing the diameter of the chimney may be beneficial to increase the lateral flow area of the chimney outflow, thus increasing the influence of the SCS on the local environmental microclimate.

Fig. 13 shows the relative humidity distribution of the air in the height direction of the chimney for different amounts of spray droplets. When the air inside the collector was heated by the ground that absorbed the sun radiation, the air temperature increased as well, and the relative humidity was correspondingly reduced; RH was only about 32.5% at the entrance of the chimney. With the complete evaporation of the spray droplets at the bottom of the chimney, the relative humidity of the air rapidly increased, and the higher amount of spray droplets leads to an increase of relative humidity, as shown in Fig. 13. At the same time, the magnitude of the increase of air relative humidity was not linear with the amount of spray droplets, but showed different sensitivities. When the amount of spray droplets was 0.1 kg/s, air relative humidity was small and increased along the height of the chimney. When the amounts of spray droplets were 0.3 kg/s and 0.4 kg/s, the air relative humidity was comparatively large, and still

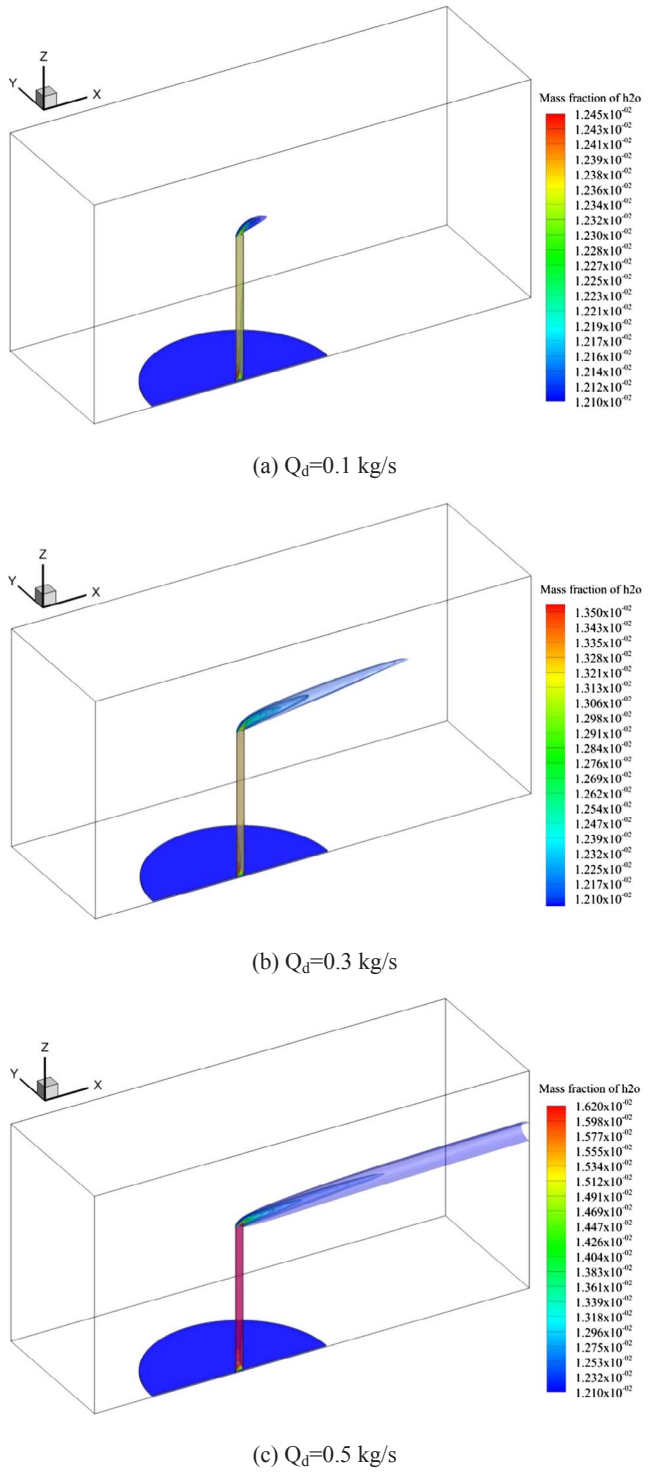

Fig. 12. Three-dimensional iso-surface distributions of the moisture content of air in the SCS under different mass flow rates of spray droplets.

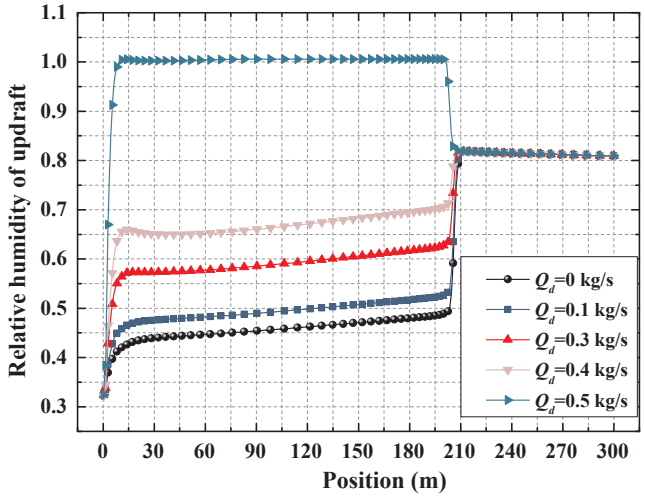

Fig. 13. Air relative humidity curves in the height direction of chimney.

increased in the direction of the chimney height. When the amount of spray droplets was 0.5 kg/s, the air relative humidity quickly climbed to near 100%, while at the same time, the water droplets evaporated and the air inside the chimney tended to be saturated. That is, when the amount of spray droplets was in the range of 0.4–0.5 kg/s, the air relative humidity inside the chimney could reach 100% in the rising process. The relative humidity was always maintained at 100% when the air increased inside the chimney and condensation phase transformation occurred. After updraft through the chimney outlet, the air relative humidity was quickly consistent with the relative humidity of the ambient in the height direction. These analyses suggest the conclusion that the evaporation of the spray droplets improved the relative humidity of the air inside the chimney and reduced the condensation height of the air moisture to a lower height, as shown in Fig. 13. When the amount of spray droplets was 0.5 kg/s, the condensation height inside the chimney was only about 15 m, while it was higher for lower amounts of spay droplets.

When the spray droplets had completely evaporated, the relative humidity of the ascending airflow in the chimney was greatly improved. In the process of increasing the thermal airflow, the enthalpy loss of the air was constantly changing into the potential energy of gravity, so that the air temperature along the way decreased, and the air relative humidity continued to increase. If the relative humidity exceeded 100%, i.e., as the condensation level was reached, saturated air would undergo condensation phase transformation. If however, the condensation level was below the chimney height, the air would condense inside the chimney. Here, it was defined that the amount of condensed water inside the chimney was:

$$Q_{cons} = Q_{inlet} + Q_d - Q_{outlet} \quad (25)$$

where Q_{inlet} represents the air mass flow rate at the inlet of collector, Q_{outlet} represents the air mass flow rate at the exit of the chimney.

Fig. 14 shows the chimney outlet flow rate and the condensed water for different amounts of droplet spray. With increasing amount of spray droplets, the chimney outlet flow rate decreased. When the amount of spray droplets had not been able to cause the air to undergo condensation phase transformation inside the chimney, the chimney outlet flow rate slightly decreased and maintained a high linear relationship. Fig. 14 shows that when the amount of spray droplets was sufficient to enable the condensation phase transformation of the humid air inside the chimney, the chimney outlet flow rate decreased sharply, and the flow performance of system was greatly weakened. After the amount of spray droplets exceeded 0.5 kg/s, the chimney outlet flow rate began to smooth and decreased; however, when the amount of spray droplets was 0.8 kg/s, the chimney outlet flow rate was very low with only about 58.6 kg/s. At the same time, air velocity was as low as 1.6 m/s; therefore, if we continued to increase the amount of spray droplets, it would potentially stop the flow of the SCS. In summary, the chimney outlet flow curve can reflect the change in the flow performance of the SCS as the amount of spray droplets increased. In the condensed water curve, when the amount of spray droplets was below 0.5 kg/s, the amount of condensed water inside the chimney was 0. I.e., the amount of spray droplets was not sufficient to cause condensation of air inside the chimney. When the amount of spray droplets was more than 0.5 kg/

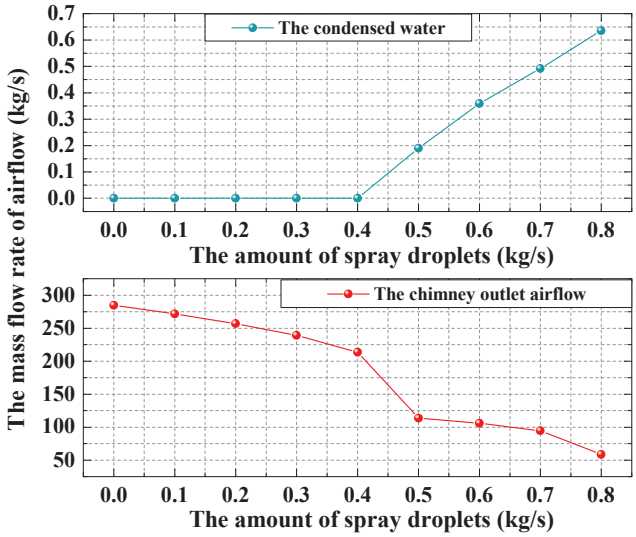

Fig. 14. Variation of chimney outlet airflow and the condensed water under different amounts of spray droplets.

s, the condensed water curve increased almost linearly with the increasing amount of spray droplets. In other words, even if the chimney system's flow performance was weakened as the amount of spray droplets increased, the amount of condensed water would still maintain a good output trend, and the condensed water would directly reflect the output performance of seawater desalination. Thus, as the amount of spray droplets increased, the amount of freshwater produced by the SCS was increasing and the rate of increase was almost constant.

To clearly describe the desalination performance of SCS, Fig. 15 shows the condensation efficiency curves of chimney system under different amounts of spray droplets. The condensation efficiency is the ratio of the condensed water to the amount of spray droplets:

$$\eta_{cons} = \frac{Q_{cons}}{Q_d} \tag{26}$$

As can be seen from Fig. 15, when the amount of spray droplets was sufficient to initiate air condensation inside the chimney, the condensation efficiency gradually increased with increasing amount of spray droplets. Although from the slope of the curve, the increase in the rate of condensation efficiency decreased with the amount of the spray droplets, but in general, the increase in the amount of spray droplets was conducive to improving the desalination efficiency of the SCS.

5. Discussion

Due to the presence of an unstable environmental lapse rate in the atmosphere, the updraft of the SCS could cool down along the chimney and spontaneously precipitate condensated water, thus providing the possibility of recovering and collecting fresh water from the air. However, the air temperature reduction or the air relative humidity increment produced by the environmental lapse rate was apparent only when the chimney was sufficiently high. In this case, it was possible to allow the updraft inside the chimney to reach the lifting condensation level, resulting in the occurrence of condensation conditions. Therefore, the actual construction of a tall chimney is a matter that poses problems of high costs and engineering feasibility, and even conducting the relevant experimental work to further validate the practical application of fresh water generation remains difficult. For this reason, although Starr and Anatii et al. [38,39] proposed to partially replicate the natural warm wet air convection process inside the chimney to recover liquid water from air in 1971, research on this issue has rarely been reported during the past decades. In our previous work [42], through the primary theoretic modeling and sensitivity analysis of the SCPPS, which combined the functions of power generation and water production, we found that the air relative humidity at the chimney inlet had a significant influence on the condensation level and the amount of condense water. More encouraging is that a few hundred meters of chimneys can even precipitate condensate water. As a result, the problem focuses on one point: a method to increase the relative humidity of the airflow when entering the chimney. In this article, the provided suggestion is the use of seawater or of brackish water. The thermal airflow at the chimney inlet is water sprayed and wetted via pumping or other means, so that the wet warm air would be brought closer to the saturated state. The idea of recovering water from the air thus transformed into a method for seawater desalination. This is expected to reduce the chimney height, thus reducing the chimney construction costs and the corresponding technical problems. Satisfyingly, the numerical results of a plant of the same size of the Manzanares pilot model were in line with expectations.

Most the existing literature presented the theoretical calculation for the SCPPS with a high chimney, and consequently tend to suffer from apparent errors. In this article, through eliminating the errors caused by various non-ideal boundary conditions, and by incorporating the ambient wind, solar radiation, environmental lapse rate, and spraying conditions, the mathematical model of water droplet evaporation and air condensation were established. In addition to analyzing the flow and temperature distributions inside and outside the SCS, the seawater desalination performance of this device was also analyzed.

The readers may pose the question whether this technique of water harvest from ambient air will lead to a reduction in natural rainfall, this resulting in related negative effects for natural environment. Actually, rainfall enhancement due to power plants cooling towers has been studied [50–52]. It can be argued that this situation is similar to the damage caused by the artificial transformation of natural reservoirs, such as irrigation and diversion channel, which began thousands of years ago. Based on the sprayed humidification solution proposed in this article, the SCS would no longer extract water from the ambient air, but from human-made saturated air originating either from seawater or brackish water, conducting to desalination. Through this sprayed humidification solution, the chimney height can be greatly reduced, and the method will be beneficial and harmless for the environment. Instead, such a SCS has the effect of improving local microclimate and enhancing local rainfall.

In fact, the atmosphere is rich in freshwater humidity, and SCS is not only a solar thermal application system able to achieve output power, but also a concept for an artificial rainfall promotion device. Particularly, on isolated islands, the only source of fresh water is desalination; therefore, the SCS can be used to achieve practical

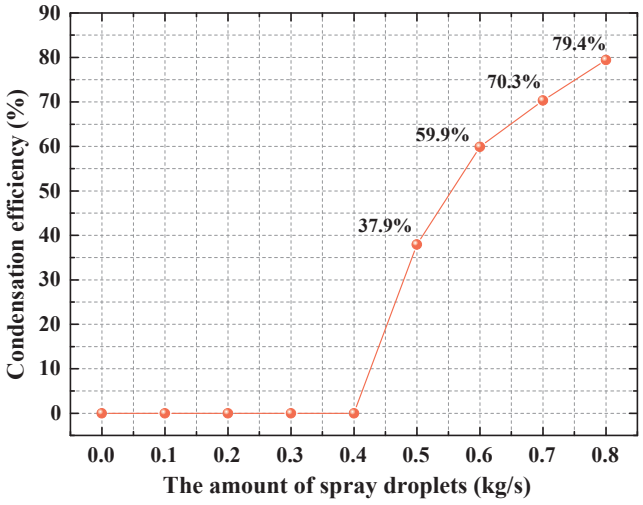

Fig. 15. Condensation efficiency curve under different amounts of spray droplets.

applications. Moreover, since it does not consume conventional energy, low pollution, low running cost, high degree of fresh water, and enhancing the local rainfall has a greater practical value; consequently, the proposed SCS for seawater desalination has a great practical value. After the preliminary research and exploration of the idea of water recovering from the air and seawater desalination for a plant of the same size of the Manzanares pilot model was conducted in this article, and future work could be gradually considered to add the time-varying ambient factors (including ambient wind and solar radiation) and a radiation model. However, two-channels within the chimney could also be built [42], to achieve power generation and seawater desalination functionality of the SCS. Finally, the most critical issue will be how to balance the efficiency of power generation and the efficiency of seawater desalination, to achieve maximum efficiency of solar energy utilization and to minimize the system cost. Moreover, constructing a small feasible experimental structure would also be a practical way for further validation from the scientific point of view.

6. Conclusion

In this article, through the idea of the introduction of seawater, the warmed airflow under the solar collector of a SCPPS was sprayed and wetted at the chimney inlet position, to achieve the purposes of reducing chimney height and system cost to recover liquid water from the air inside the chimney by partially replicating a natural warm wet air convection process. The main conclusions are as follows:

(1) When the warmed airflow was sprayed and humidified, the air temperature inevitably decreased, regardless of whether the air condensed inside the chimney, resulting in a decrease in the temperature difference between the system and the ambient, and a weakening of the driving force and the system's flow performance.
(2) When the ambient crosswind conditions remain constant, a higher amount of spray droplets will increase the mass fraction of water in the air, and the impact on the local environment microclimate; evaporation of the spray droplets improved the relative humidity of the air in the chimney, and reduced the condensation level to a lower height.
(3) With increasing amount of spray droplets, the output water of SCS increased, which was conducive to improving the desalination efficiency of the SCS.

Acknowledgements

This study was supported by the National Natural Science Foundation of China (No. 51778511), Key Project of ESI Discipline Development of Wuhan University of Technology (WUT No. 2017001), the Science Challenge Project (No. TZ2017003), and the Scientific Research Foundation of Wuhan University of Technology (No. 40120237).

Author Contributions

Tingzhen Ming and Tingrui Gong contributed equally to the work.

References

[1] Haaf W, Friedrich K, Mayr G, Schlaich J. Solar chimneys part I: principle and construction of the pilot plant in Manzanares. Int J Solar Energy 1983;2:3–20.
[2] Haaf W. Solar chimneys: part ii: preliminary test results from the Manzanares pilot plant. Int J Sustain Energ 1984;2:141–61.
[3] McMahon T. Historical Crude Oil Prices https://inflationdata.com/Inflation/Inflation_Rate/Historical_Oil_Prices_Table.asp; 2015 [accessed 15.08.17].
[4] Zhou XP, Wang F, Ochieng RM. A review of solar chimney power technology. Renew Sust Energ Rev 2010;14:2315–38.
[5] Zhou X, Xu Y. Solar updraft tower power generation. Sol Energy 2016;128:95–125.
[6] Bonnelle D. Solar chimney, water spraying energy tower, and linked renewable energy conversion devices: presentation, criticism and proposals. PhD: University Claude Bernard-Lyon; 2004.
[7] Krätzig WB. Physics, computer simulation and optimization of thermo-fluidmechanical processes of solar updraft power plants. Sol Energy 2013;98:2–11.
[8] Technology Overview. Enviromission, http://www.enviromission.com.au/EVM/content/technology_technologyover.html; 2015.
[9] von Backström TW, Harte R, Höffer R, Krätzig W, Kröger D, Niemann H, et al. State and recent advances in research and design of solar chimney power plant technology. VGB Powertech 2008;88:64–71.
[10] Pretorius JP. Optimization and control of a large-scale solar chimney power plant. Stellenbosch: University of Stellenbosch; 2007.
[11] Pasumarthi N, Sherif SA, Pasumarthi N, Sherif SA. Experimental and theoretical performance of a demonstration solar chimney model—Part I: mathematical model development. Int J Energy Res 1998;22:277–88.
[12] Padki MM, Sherif SA. On a simple analytical model for solar chimneys. Int J Energy Res 1999;23:345–9.
[13] Tingzhen M, Wei L, Guoliang X. Analytical and numerical investigation of the solar chimney power plant systems. Int J Energy Res 2006;30:861–73.
[14] Ming T, Wang X, Richter RKD, Liu W, Wu T, Pan Y. Numerical analysis on the influence of ambient crosswind on the performance of solar updraft power plant system. Renew Sust Energ Rev. 2012;16:5567–83.
[15] Ming T, Richter RK, Meng F, Pan Y, Liu W. Chimney shape numerical study for solar chimney power generating systems. Int J Energy Res 2013;37:310–22.
[16] Bernardes MAD, Voss A, Weinrebe G. Thermal and technical analyses of solar chimneys. Sol Energy 2003;75:511–24.
[17] Nizetic S, Klarin B. A simplified analytical approach for evaluation of the optimal ratio of pressure drop across the turbine in solar chimney power plants. Appl Energy 2010;87:587–91.
[18] Krätzig WB. Solar updraft power technology: Fighting global warming and rising energy costs. J Technol Innov Renew Energy 2015;4:52–64.
[19] Shirvan KM, Mirzakhanlari S, Mamourian M, Kalogirou SA. Optimization of effective parameters on solar updraft tower to achieve potential maximum power output: A sensitivity analysis and numerical simulation. Appl Energy 2017;195:725–37.
[20] Patel SK, Prasad D, Ahmed MR. Computational studies on the effect of geometric parameters on the performance of a solar chimney power plant. Energy Convers Manage 2014;77:424–31.
[21] Maia CB, Ferreira AG, Valle RM, Cortez MFB. Theoretical evaluation of the influence of geometric parameters and materials on the behavior of the airflow in a solar chimney. Comput Fluids 2009;38:625–36.
[22] Maia CB, Castro Silva JO, Cabezas-Gómez L, Hanriot SM, Ferreira AG. Energy and exergy analysis of the airflow inside a solar chimney. Renew Sust Energ Rev 2013;27:350–61.
[23] Gholamalizadeh E, Mansouri S. A comprehensive approach to design and improve a solar chimney power plant: a special case–Kerman project. Applied Energy 2013;102:975–82.
[24] Hu S, Leung DY, Chan JC. Numerical modelling and comparison of the performance of diffuser-type solar chimneys for power generation. Appl Energy 2017.
[25] de Richter R, Ming T, Davies P, Liu W, Caillol S. Removal of non-CO2 greenhouse gases by large-scale atmospheric solar photocatalysis. Prog Energy Combust Sci 2017;60:68–96.
[26] Gong T, Ming T, Huang X, de Richter RK, Wu Y, Liu W. Numerical analysis on a solar chimney with an inverted U-type cooling tower to mitigate urban air pollution. Sol Energy 2017;147:68–82.
[27] Zheng Z, He S. Modeling and characteristics analysis of hybrid cooling-tower-solar-chimney system. Energy Convers Manage 2015;95:59–68.
[28] Lee D-S, Hung T-C, Lin J-R, Zhao J. Experimental investigations on solar chimney for optimal heat collection to be utilized in organic Rankine cycle. Appl Energy 2015;154:651–62.
[29] Ferreira AG, Maia CB, Cortez MFB, Valle RM. Technical feasibility assessment of a solar chimney for food drying. Sol Energy 2008;82:198–205.
[30] Li Y, Liu S. Experimental study on thermal performance of a solar chimney combined with PCM. Appl Energy 2014;114:172–8.
[31] Ninic N, Nizetic S. Elementary theory of stationary vortex columns for solar chimney power plants. Sol Energy 2009;83:462–76.
[32] Yu Y, Li H, Niu F, Yu D. Investigation of a coupled geothermal cooling system with earth tube and solar chimney. Appl Energy 2014;114:209–17.
[33] Kroger DG, Blaine D. Analysis of the driving potential of a solar chimney power plant. SAI MechE R & D J 1999;15:85–94.
[34] Pretorius JP, Kröger DG. Incorporating vegetation under the collector roof of a solar chimney power plant. R & D J South Afr Instit Mech Eng 2008;24:3–11.
[35] VanReken TM, Nenes A. Cloud formation in the plumes of solar chimney power generation facilities: a modeling study. J SolEnergy Eng 2009;131:011009.
[36] Kashiwa B, Kashiwa CB. The solar cyclone: A solar chimney for harvesting atmospheric water. Energy 2008;33:331–9.
[37] Squires P, Turner J. An entraining jet model for cumulo-nimbus updraughts. Tellus 1962;14:422–34.
[38] Starr VP, Anati DA. Experimental engineering procedure for the recovery of liquid water from the atmospheric vapor content. Pure Appl Geophys 1971;86:205–8.
[39] Starr VP, Anati DA, Gaut NE. Controlled atmospheric convection in an engineered structure. Nord Hydrol 1972;3:1–21.
[40] Rogers P. Nation's largest ocean desalination plant goes up near San Diego; Future of the California coast? http://www.mercurynews.com/science/ci_25859513/nations-largest-ocean-desalination-plant-goes-up-near; 2014.
[41] Ming T, Gong T, de Richter RK, Liu W, Koonsrisuk A. Freshwater generation from a solar chimney power plant. Energy Convers Manage 2016;113:189–200.
[42] Ming T, Gong T, de Richter RK, Wu Y, Liu W. A moist air condensing device for

sustainable energy production and water generation. Energy Convers Manage 2017;138:638–50.
[43] Zhou XP, Yang JK, Xiao B, Shi XY. Special climate around a commercial solar chimney power plant. J Energy Eng-Asce 2008;134:6–14.
[44] Zhou X, Xiao B, Liu W, Guo X, Yang J, Fan J. Comparison of classical solar chimney power system and combined solar chimney system for power generation and sea-water desalination. Desalination 2010;250:249–56.
[45] Reynolds WC. Thermodynamic properties in SI: Graphs, tables, computational equations for forty substances. University Departement of Mechanical Engineering; 1979.
[46] Cermak J. Applications of fluid mechanics to wind engineering—a Freeman Scholar lecture. J Fluids Eng 1975;97:9–38.
[47] Pastohr H, Kornadt O, Gürlebeck K. Numerical and analytical calculations of the temperature and flow field in the upwind power plant. Int J Energy Res 2004;28:495–510.
[48] Sangi R, Amidpour M, Hosseinizadeh B. Modeling and numerical simulation of solar chimney power plants. Sol Energy 2011;85:829–38.
[49] Xu G, Ming T, Pan Y, Meng F, Zhou C. Numerical analysis on the performance of solar chimney power plant system. Energy Convers Manage 2011;52:876–83.
[50] Niewiadomski M, Haman KE. The rainfall enhancement by washout of cooling tower plumes: A numerical experiment. Atmos Environ 1967;18(1984):2483–9.
[51] Selvam A, Manohar G, Murty BVR. Rainfall variations around a thermal power station. Atmos Environ 1967;10(1976):963–8.
[52] Dana M, Wolf M. Rainfall enhancement due to washout of cooling tower condensate. Report PNL-2500 Battelle Pacific Northwest Labs., Richland, WA (USA) http://www.iaea.org/inis/collection/NCLCollectionStore/_Public/10/444/10444869.pdf; 1978 [accessed 15.08.17].